Multistate Equilibrium Unfolding of *Escherichia coli* Dihydrofolate Reductase: Thermodynamic and Spectroscopic Description of the Native, Intermediate, and Unfolded Ensembles†

Roxana M. Ionescu, Virginia F. Smith, John C. O'Neill, Jr., and C. Robert Matthews*

Department of Chemistry, Life Sciences Consortium and Center for Biomolecular Structure and Function, The Pennsylvania State University, University Park, Pennsylvania 16802

Received March 6, 2000; Revised Manuscript Received May 25, 2000

ABSTRACT: The thermodynamic and spectroscopic properties of a cysteine-free variant of *Escherichia coli* dihydrofolate reductase (AS-DHFR) were investigated using the combined effects of urea and temperature as denaturing agents. Circular dichroism (CD), absorption, and fluorescence spectra were recorded during temperature-induced unfolding at different urea concentrations and during urea-induced unfolding at different temperatures. The first three vectors obtained by singular-value decomposition of each set of unfolding spectra were incorporated into a global analysis of a unique thermodynamic model. Although individual unfolding profiles can be described as a two-state process, a simultaneous fit of 99 vectors requires a three-state model as the minimal scheme to describe the unfolding reaction along both perturbation axes. The model, which involves native (N), intermediate (I), and unfolded (U) states, predicts a maximum apparent stability, $\Delta G°_{NU}$, of 6 kcal mol^{-1} at 15 °C, an apparent m_{NU} value of 2 kcal mol^{-1} M^{-1}, and an apparent heat capacity change, ΔC_{p-NU}, of 2.5 kcal mol^{-1} K^{-1}. The intermediate species has a maximum stability of approximately 2 kcal mol^{-1} and a compactness closer to that of the native than to that of the unfolded state. The population of the intermediate is maximal (∼70%) around 50 °C and falls below the limits of detection of ≥2 M urea or at temperatures of <35 or >65 °C. The fluorescence properties of the equilibrium intermediate resemble those of a transient intermediate detected during refolding from the urea-denatured state, suggesting that a tryptophan-containing hydrophobic cluster in the adenosine-binding domain plays a key role in both the equilibrium and kinetic reactions. The CD spectroscopic properties of the native state reveal the presence of two principal isoforms that differ in ligand binding affinities and in the packing of the adenosine-binding domain. The relative populations of these species change slightly with temperature and do not depend on the urea concentration, implying that the two native isoforms are well-structured and compact. Global analysis of data from multiple spectroscopic probes and several methods of unfolding is a powerful tool for revealing structural and thermodynamic properties of partially and fully folded forms of DHFR.

The access to protein sequences provided by the rapidly expanding genomic databases makes the understanding of the relationship between the amino acid sequence of a protein and its three-dimensional structure an imperative. Given that the sequence contains all of the information required to access the native, functional form (*1*), insights can presumably be obtained from the study of partially folded kinetic and/or equilibrium intermediates that appear during the folding reaction. Both equilibrium and kinetic approaches are vital for defining the energy surface of folding, because the discrimination among different kinetic models may not be possible without a consideration of equilibrium data (*2*). For example, the combined approach can be used to determine whether a partially folded species populated at equilibrium corresponds to a direct precursor of the native state, i.e., an on-pathway intermediate, or whether it represents a misfolded species that must unfold before accessing the native form, i.e., an off-pathway intermediate. These issues and others are often difficult to resolve because equilibrium intermediates, if they exist, can be harder to detect and/or to characterize than their kinetic counterparts.

There are three classic tests for multistate equilibrium behavior for protein folding reactions. The first is examination of the shape of the unfolding transition curve obtained by any relevant perturbation, e.g., temperature, chemical denaturant, pH, etc. Deviation from a simple sigmoidal dependence, i.e., an inflection, provides direct evidence for the presence of one or more thermodynamic states in addition to the native and unfolded states. However, a sigmoidal transition does not necessarily exclude the existence of intermediate, partially folded states (*3*). The second is comparison of the unfolding reaction detected by two or more techniques that are sensitive to different structural properties. Coincidence of the normalized transitions provides strong support for a two-state process. Noncoincidence is more difficult to interpret because it may reflect either the presence of distinct partially folded forms or the existence of broad

† This work was supported by National Science Foundation Grant MCB-9604678 to C.R.M. V.F.S. was supported in part by an NIH Postdoctoral Fellowship (GM19401).

* To whom correspondence should be addressed. E-mail: crm@psu.edu. Phone: (814) 865-8859. Fax: (814) 863-8403.

10.1021/bi000511y CCC: $19.00 © 2000 American Chemical Society
Published on Web 07/12/2000

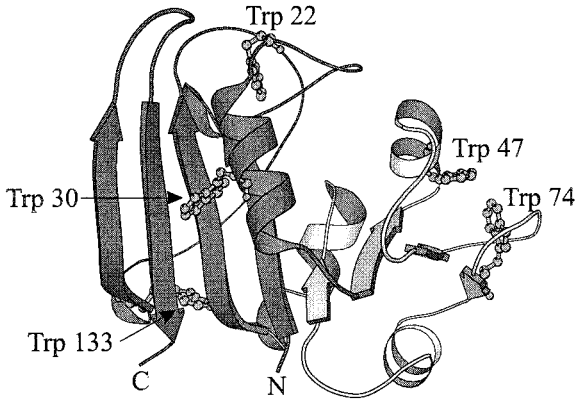

FIGURE 1: Ribbon diagram of *E. coli* DHFR (Protein Data Bank entry 1rx3). The two domains (*9*) are shown in different shades of gray: dark gray, the loop domain (residues 1−37 and 107−159); and light gray, the adenosine-binding domain (residues 38−106). In a ball-and-stick representation are shown the five tryptophan residues at positions 22, 30, 47, 74, and 133. This figure was generated using the program Molscript (*59*).

ensembles of native and/or unfolded structures (*4*). The third is comparison of the van't Hoff and calorimetric enthalpies for the thermal unfolding reaction. Equivalence of the two enthalpies is a necessary but not sufficient condition for a two-state unfolding reaction (*5*). Although these tests are useful in eliminating incorrect equilibrium models, the extraction of quantitative estimates of thermodynamic and spectroscopic properties of any stable intermediates may be difficult. Fortunately, the development of global analysis and automated data collection (*6*−*8*) can provide access to this information.

Dihydrofolate reductase (DHFR)[1] from *Escherichia coli*, a 159-residue amino acid protein containing a nucleotide-binding domain (*9*), provides an interesting test case for a global equilibrium analysis. DHFR catalyzes the reduction of 7,8-dihydrofolate to 5,6,7,8-tetrahydrofolate in the presence of NADPH. The binding sites for the substrate and cofactor delimit two domains in the folded structure, the adenosine-binding domain and the loop domain (Figure 1) (*9*). The secondary structural elements, four helices and an eight-stranded β-sheet, are assembled into a complex global topology in which the sequence of the adenosine-binding domain (residues 38−106) is embedded within the discontinuous sequence of the loop domain (residues 1−37 and 107−159). Three of the five tryptophan residues in *E. coli* DHFR (Trp 22, Trp 30, and Trp 133) are located in the loop domain, and two (Trp 47 and Trp 74) are located in the adenosine-binding domain. Mutational analysis demonstrated that Trp 74 makes a distinct spectroscopic contribution to the far-UV CD (*10*) and fluorescence (*11*) properties of the protein.

[1] Abbreviations: Abs_{292}, absorption measured at 292 nm; ACU and ACV, autocorrelation coefficients of the U and V vectors from SVD, respectively; AS-DHFR, C85A/C152S cysteine-free double mutant of dihydrofolate reductase; CD, circular dichroism; DHFR, dihydrofolate reductase; Flu_{370}, fluorescence measured at 370 nm; N, I, and U, native, intermediate, and unfolded states involved in AS-DHFR unfolding, respectively; N_{NB}, part of the native state ensemble with low affinity for $NADP^+$; N_B, part of the native state ensemble with high affinity for $NADP^+$; $[\theta]_{222}$, mean residue ellipticity measured at 222 nm; SE-DHFR, C85S/C152E cysteine-free double mutant of DHFR; SVD, singular-value decomposition; WT-DHFR, wild-type dihydrofolate reductase.

Previous equilibrium studies of the urea-induced unfolding of wild-type DHFR at 15 °C (*12*) using CD, absorbance (Abs), and fluorescence (Flu) spectroscopy revealed that the reaction is described well by a two-state model. In contrast, WT-DHFR has a very complex kinetic response when urea is used as a denaturing agent. The observation of six kinetic phases in refolding and at least three in unfolding was explained by a parallel four-channel model, in which two classes of partially folded intermediates are populated in the refolding process (*13*, *14*). The complexity of the system is further highlighted by ligand binding kinetics (*15*) and two-dimensional ^{1}H NMR (*16*) that reveal at least two slowly interconverting conformers of the native apoprotein present in solution. The multiple native conformers play prominent roles in both unfolding and refolding reactions.

The equilibrium thermal unfolding reaction of DHFR, unlike urea denaturation, is not described well by a two-state model. Differential scanning calorimetry on G-DHFR (a mutant of *E. coli* DHFR with Cys 152 replaced with Glu and three additional residues at the C-terminus) revealed that the temperature-induced unfolding occurs with a significant population of an equilibrium intermediate (*17*). A spectroscopic study of WT-DHFR (*18*) also found that the temperature-induced unfolding occurs with an equilibrium intermediate. However, these conclusions and the thermodynamic parameters reported must be tempered by the known irreversibility of DHFR to thermal unfolding (*17*, *19*). Recently, the presence of an intermediate in the thermal unfolding of WT-DHFR has also been inferred from the reversible urea-induced unfolding at moderate temperatures (*20*). In contrast to the previous studies, this additional state was attributed to the minor, nonligand binding conformer in the apoenzyme.

The goal of this study was to provide a quantitative analysis of the thermodynamic properties of *E. coli* DHFR by performing a systematic investigation using multiple spectroscopic probes (CD, absorbance, and fluorescence) along two perturbation axes, urea and temperature. AS-DHFR, a cysteine-free variant of *E. coli* DHFR, in which the two non-disulfide-bridged cysteine residues have been replaced with alanine and serine, was selected because it presents a highly reversible thermal unfolding reaction and because its thermodynamic and kinetic properties and enzymatic activity are similar to those of WT-DHFR (*19*). Global analysis of these data shows that a partially folded form, distinct from the two native conformers, plays a significant role in the equilibrium folding reaction and resembles a transient folding intermediate.

MATERIALS AND METHODS

Protein Preparation. The construction and expression of a plasmid containing the gene for AS-DHFR has been described elsewhere (*19*). The protein concentration was determined using the extinction coefficient of WT-DHFR at 280 nm [$\epsilon_{280} = 3.11 \times 10^4$ M^{-1} cm^{-1} (*12*)]. Protein concentrations used in equilibrium unfolding experiments were approximately 3, 5, and 10 μM for Flu, CD, and Abs measurements, respectively. Previous experiments have shown that, in this concentration range, the equilibrium and kinetic properties of DHFR are independent of protein concentration (*12*, *19*). The buffer contained 10 mM potassium phosphate (pH 7.8) and 0.2 mM K_2EDTA.

Reagents. Ultrapure urea was purchased from ICN Biomedicals, Inc. (Aurora, OH) and purified further with a mixed-bed ion-exchange resin (AG 501-X8, Bio-Rad Laboratories, Hercules, CA). Urea concentrations were determined from refractive index measurements (*21*). The oxidized form of nicotinamide adenine dinucleotide phosphate ($NADP^+$) was purchased from Sigma (St. Louis, MO). The concentration of $NADP^+$ was determined using a molar extinction coefficient at 260 nm (ϵ_{260}) of 1.8×10^4 M^{-1} cm^{-1} (Sigma).

Equilibrium Unfolding Studies. Fluorescence emission spectra were recorded on an AVIV ATF 105 fluorometer. The excitation wavelength was 295 nm, and the emission was recorded from 310 to 510 nm, with a 1 nm step size and a 1 s integration time. CD measurements were taken on an AVIV 62DS spectrophotometer by recording spectra at 1 nm increments between 221 and 260 nm and using an integration time of 3 s. The high absorbance of urea made it impossible to record spectra below 221 nm in the 1 cm $\times$ 1 cm cells used for the automatic titration experiments (see below). Absorption spectra were recorded on an AVIV 14DS UV-vis spectrophotometer in 1 nm increments between 260 and 310 nm and using an integration time of 4 s. The sample temperature was controlled by a thermoelectric cell holder in each instrument.

Temperature- and urea-induced unfolding experiments were automated to enhance the accuracy of the measurements. For CD and Abs measurements, an auxiliary computer coordinated the addition of denaturant or the temperature variation with the data acquisition. For Flu measurements, the instrument software controlled the data recording and the stepwise change in the denaturant concentration. The performance of the automatic titrator (Microlab 500 series) was checked at the end of each experiment. The differences between the expected and measured values of the final urea concentration in the cell were less than 2%. To ensure that equilibrium was reached before data acquisition, the equilibration times prior to measurements were adjusted for various solvent conditions and were based upon the known kinetic properties of WT-DHFR (*13*). Equilibration times varied between 2 and 15 min, with longer times at low temperatures or in the transition region of the urea-induced unfolding. The reversibility of the process in temperature-induced unfolding was verified by comparing, for each urea concentration, CD unfolding profiles obtained by increasing the temperature to the profiles obtained by decreasing the temperature. Although good recovery ($\sim$95%) of the signal at room temperature was obtained after the protein was kept at 70 °C in 2.5 M urea for 15 min, AS-DHFR undergoes irreversible changes after long exposures to high temperatures in the presence of denaturant. Urea titrations at 70 °C and temperature melts in 6 M urea were monitored by CD at only one wavelength, 225 nm, to avoid long exposures of the protein to harsh solvent conditions. Moreover, the analysis of temperature-induced unfolding data in the presence of urea was limited to temperatures of $<$70 °C to minimize contributions from irreversible processes. The high degree of reversibility of DHFR to urea-induced unfolding at different temperatures has been reported elsewhere (*20*).

Ultracentrifugation. Equilibrium sedimentation experiments were performed on a Beckman XL-I analytical ultracentrifuge. Absorbance at 280 nm as a function of the radial distance was measured in an eight-cell rotor rated for 50 000 rpm. All experiments were carried out at 40 °C. Radial scans were recorded at 25 000 rpm after an equilibration time of 24 h. Two additional scans were performed 2 and 4 h after the equilibration delay. The same protocol was used for runs at 35 000 rpm, with the difference being that the initial equilibration time was 12 h. The final buffer contained 20 mM potassium phosphate (pH 7.8), 0.2 mM K_2EDTA, and 100 mM KCl. The protein concentrations used in equilibrium sedimentation experiments were 5, 10, and 20 μM. To determine the molecular weight, data were analyzed with the program Windows NONLIN (*23*, *24*) assuming ideal conditions. The partial specific volume of the protein (0.7412 mL g^{-1}) and the density of the buffer (0.9994 g mL^{-1}) were calculated using the program SEDNTERP (*25*, *26*).

Ligand Binding Experiments. $NADP^+$ binding to native AS-DHFR was measured on an AVIV stopped-flow fluorescence instrument, model 202, with a dead time of 5 ms. The excitation wavelength was 290 nm, and the emission was measured using a cutoff filter at 320 nm. The final protein and $NADP^+$ concentrations in the mixing cell were 1 and 100 μM, respectively. Previous studies on *L. casei* (*27*) and *E. coli* (*28*) DHFR at 25 and 10 °C, respectively, reported a dissociation constant for $NADP^+$ of $\sim$15 μM for both enzymes; the on-rate constant for the *L. casei* enzyme is about 8×10^6 M^{-1} s^{-1}. $NADP^+$ binding occurs in two phases. The fast phase corresponds to the binding to a native form with a high affinity for $NADP^+$. The slow phase, which does not depend on ligand concentration, represents the interconversion of the remaining native protein from the nonbinding to the binding form. For the $NADP^+$ concentration used in these experiments, the fast phase occurs in about 1 ms, i.e., within the dead time of the instrument. The fractions of the $NADP^+$ binding and nonbinding species were determined from the relative amplitudes of the fast (occurring in the instrument dead time) and slow binding phases (*20*). The fraction of the two species was determined at 15, 20, 25, and 30 °C in the absence of urea. In a different set of experiments, the temperature was kept constant at 20 °C, and $NADP^+$ binding was monitored in the presence of 0, 0.5, 1, 1.5, and 2 M urea.

Data Analysis. Singular-value decomposition (SVD) analysis was performed using in-house software. The method (*29*) consists of decomposing a set of spectra recorded at different denaturant values into a minimum number of independent basis vectors, each with its denaturant dependence and associated spectra. The SVD analysis is model-independent and permits a cursory examination of a large data set to determine whether the signals recorded at different wavelengths respond in a concerted manner to denaturant changes. Because SVD provides vectors with a higher signal/noise ratio than the raw data, the method engenders more confidence in the thermodynamic parameters retrieved from the analyses. The minimal number of states required for an accurate description of the unfolding process was determined by inspecting the weights and the autocorrelation coefficients for the spectral properties (ACU) and for the denaturant dependence (ACV) of the vectors resulting from SVD analysis. Because the changes in Abs and Flu upon unfolding are rather small, the SVD analysis for these spectroscopic probes was performed on the difference spectra, i.e., on the spectra from which the initial spectrum (corresponding to

5 °C or 0 M urea) had been subtracted. The unfolded baselines of the SVD vectors for the Flu and Abs transitions display some curvature at high urea concentrations (an effect also observed for *N*-acetyltryptophanamide, data not shown); therefore, the analysis of unfolding profiles versus urea was limited to 5.5 M urea for Flu and to 6 M urea for Abs.

Multiple unfolding profiles were simultaneously fit by global analysis to extract the relevant thermodynamic parameters. In the fitting procedure, global (common to all data sets) and local (specific to individual profiles) parameters are iteratively adjusted until one obtains a satisfactory fit of the data. Other examples of global analysis applied to the protein folding problem can be found elsewhere (*6*−*8*).

A total of 99 vectors, representing the first three basis vectors obtained in each unfolding experiment, were considered for global analysis. The data pool was formed by temperature-induced unfolding at six urea concentrations measured by CD or Abs (3 basis vectors × 6 urea concentrations × 2 signals = 36 vectors) and by urea-induced unfolding at seven temperatures measured by CD, Abs, and Flu (3 basis vectors × 7 temperatures × 3 signals = 63 vectors). The temperature-induced unfolding assessed by Flu was not considered in the data analysis because the temperature dependence of the baselines was too large to permit reliable conclusions (see Results).

The equations for a two-state analysis have been described elsewhere (*30*). The three-state model used in the global analysis was

$$\mathrm{N} \rightleftarrows \mathrm{I} \rightleftarrows \mathrm{U} \tag{1}$$

where N, I, and U are the native, intermediate, and unfolded states, respectively. The two equilibrium constants describing the system are defined as follows:

$$K_{\mathrm{NI}} = \frac{[\mathrm{I}]}{[\mathrm{N}]};\ K_{\mathrm{IU}} = \frac{[\mathrm{U}]}{[\mathrm{I}]} \tag{2}$$

The partition function Q is defined as

$$Q = 1 + K_{\mathrm{NI}} + K_{\mathrm{NI}}K_{\mathrm{IU}} \tag{3}$$

and the fraction of each species is

$$f_{\mathrm{N}} = \frac{1}{Q};\ f_{\mathrm{I}} = \frac{K_{\mathrm{NI}}}{Q};\ f_{\mathrm{U}} = \frac{K_{\mathrm{NI}}K_{\mathrm{IU}}}{Q} \tag{4}$$

The free energy change corresponding to each equilibrium constant is assumed to have the following dependence on temperature and urea:

$$\Delta G^{\circ}_{\mathrm{i}}(T,\mathrm{urea}) = T_{\mathrm{m,i}}\Delta S^{\circ}_{\mathrm{m,i}} + \Delta C_{p-\mathrm{i}}(T - T_{\mathrm{m,i}}) - T\left(\Delta S^{\circ}_{\mathrm{m,i}} + \Delta C_{p-\mathrm{i}} \ln\frac{T}{T_{\mathrm{m,i}}}\right) - m_{\mathrm{i}}[\mathrm{urea}] \tag{5}$$

where $\Delta S^{\circ}_{\mathrm{m}}$ is the entropy difference at the melting temperature T_{m}, ΔC_p is the heat capacity difference, m is a parameter describing the effect of urea on the free energy of unfolding, and i is an index for each transition, N ⇄ I or I ⇄ U. Because four thermodynamic parameters ($\Delta S^{\circ}_{\mathrm{m}}$, T_{m}, ΔC_p, and m) are used for the description of each equilibrium constant, the scheme described in eq 1 contains a total of eight global fitting parameters.

Several assumptions were made in the application of a thermodynamic model to the unfolding of AS-DHFR over two perturbation axes. First, the temperature- and urea-induced unfolded states were considered to be part of the same thermodynamic ensemble. This assumption, which is consistent with the behavior of many other proteins (*31*−*39*), is supported by the absence of a cooperative transition when the temperature-induced unfolded species was titrated with urea or when the protein unfolded in 6 M urea was heated to 70 °C (data not shown). Second, the free energy of unfolding was assumed to depend linearly on the denaturant concentration (*31*, *33*, *40*). Third, ΔC_p and m were considered to be independent of urea or temperature over the range that was examined (*31*−*33*, *36*, *38*, *39*, *41*−*43*). Because ΔC_p and m are both correlated with the number of residues in a protein (*44*), it was assumed that $\Delta C_{p-\mathrm{NI}} = m_{\mathrm{NI}}/m_{\mathrm{NU}} \times \Delta C_{p-\mathrm{NU}}$, where m_{NI}, m_{NU}, and $\Delta C_{p-\mathrm{NU}}$ were global fitting parameters. Without this constraint, it was not possible to obtain reliable estimates of the heat capacity changes for individual steps in the three-state model.

Other assumptions are directly related to the spectroscopic properties of the protein. The measured signal, Y, contains contributions from each species

$$Y = f_{\mathrm{N}}Y_{\mathrm{N}} + f_{\mathrm{I}}Y_{\mathrm{I}} + f_{\mathrm{U}}Y_{\mathrm{U}} \tag{6}$$

where f_{j} represents the fraction of species j (as defined in eq 4) and Y_{j} is the molar signal of species j. The signals corresponding to the native and the unfolded state were considered as local fitting parameters that have a linear dependence on denaturant:

$$Y_{\mathrm{j}} = Y_{\mathrm{j}}^{\circ} + \alpha_{\mathrm{j}}[\mathrm{urea}] \tag{7}$$

where Y_{j}° is the molar signal of species j at zero denaturant and α_{j} is a "slope" describing the dependence of signal Y_{j} on denaturant concentration. In the denaturant range where the unfolding process does not make a significant contribution to changes in the spectroscopic signal, eq 7 describes the "baseline" of species j. The signal of the intermediate, Y_{I}, was described by the nondimensional parameter Z

$$Y_{\mathrm{I}} = (1 - Z)Y_{\mathrm{N}} + ZY_{\mathrm{U}} \tag{8}$$

where Z was considered to be a global fitting parameter for a representative vector of each type of signal, e.g., the first vector obtained from the SVD of CD spectra, and was assumed to be independent of denaturant concentration. The use of eq 8 reduces by 1 the number of spectroscopic fitting parameters per unfolding profile; eq 8 is equivalent to the assumption that the molar signal of I and its corresponding slope satisfy the relationship

$$Z = \frac{Y_{\mathrm{I}}^{\circ} - Y_{\mathrm{N}}^{\circ}}{Y_{\mathrm{U}}^{\circ} - Y_{\mathrm{N}}^{\circ}} = \frac{\alpha_{\mathrm{I}} - \alpha_{\mathrm{N}}}{\alpha_{\mathrm{U}} - \alpha_{\mathrm{N}}} \tag{9}$$

The thermodynamic and spectroscopic parameters were optimized in global fits by nonlinear least-squares analysis using the Marquardt−Levenburg algorithm in Savuka version 5.0, an in-house software package.

RESULTS

Temperature-Induced Unfolding. Representative thermal unfolding profiles of AS-DHFR obtained by monitoring the

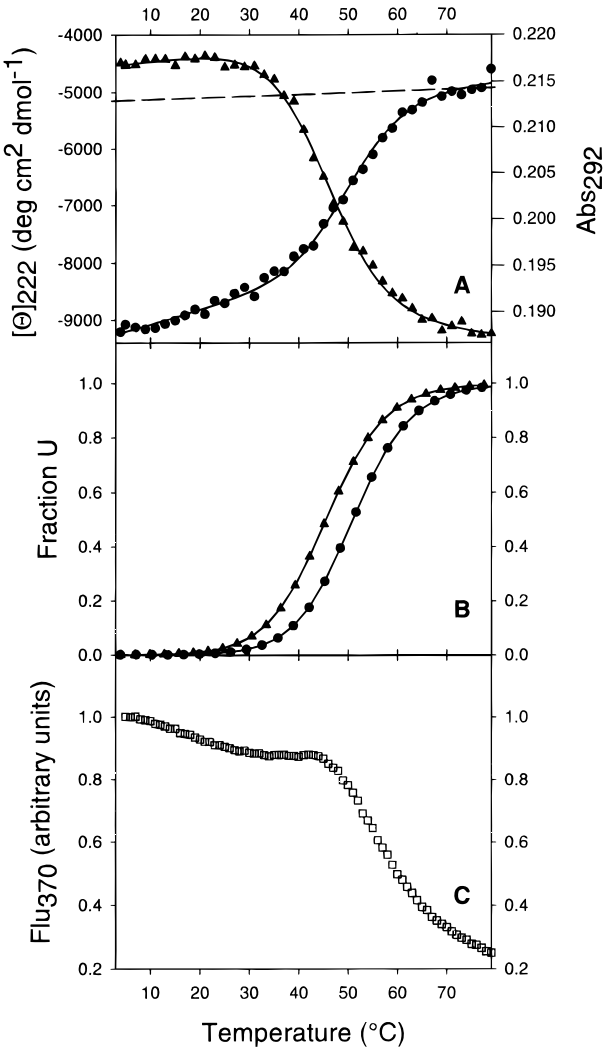

FIGURE 2: (A) Temperature-induced unfolding of AS-DHFR monitored by CD (●) and Abs (▲) spectroscopy. The solid lines represent the fitting curves obtained by separately analyzing the unfolding profiles with a two-state model. The dashed line represents the linear extrapolation of the CD signal of the unfolded state to low temperatures. The results are shown only at 222 nm for CD and 292 nm for Abs, but an expanded wavelength range (221−260 nm for CD and 260−310 nm for Abs) was studied in each case. (B) Fraction of the unfolded species obtained from the two-state fits for CD data at 222 nm (●) and Abs data at 292 nm (▲). (C) Temperature-induced unfolding of AS-DHFR monitored by Flu at 370 nm. The protein concentration was 5 μM for CD, 10 μM for Abs, and 3 μM for Flu measurements. The buffer was 10 mM potassium phosphate (pH 7.8) with 0.2 mM K_2EDTA.

CD, Abs, and Flu are shown in Figure 2. The profiles exhibit small linear variations of the signal from 5 to 35 °C that correspond to native baselines, sigmoidal changes that reflect a cooperative unfolding between 40 and 70 °C, and unfolded baseline regions of >70 °C. Although CD and Abs individually appear to monitor a two-state reaction (the solid lines in Figure 2A represent a fit using a two-state model), comparison of the plots of the fraction of unfolded species (Figure 2B) shows that the transitions are not coincident. The midpoint of transition, T_m, monitored by Abs at 292 nm is about 5 °C lower than that obtained from the CD signal at 222 nm. Clear deviations from a two-state process are also seen in the Flu data (Figure 2C), where the inflection in the signal around 45 °C is contrary to the expectation for a simple interconversion between native and unfolded forms. Similar behavior in fluorescence has been reported for the temperature-induced unfolding of WT-DHFR (*18*).

The unfolding profiles shown in Figure 2 are only slices of a larger spectral domain recorded for each signal. More convincing arguments about deviations from a two-state process were developed by analyzing full spectra using the singular-value decomposition (SVD) analysis (*29*). The method involves decomposing the unfolding data (amplitude of the signal versus wavelength and denaturant) into a set of basis vectors, each vector being characterized by its spectrum and its response to perturbant. The decomposition routine also provides a weight for each vector that reflects its contribution to the overall process.

SVD analysis of CD spectra for the temperature-induced unfolding in the absence of urea revealed three significant basis vectors, as judged by the normalized weights and the autocorrelation coefficients. The first and second vectors comprise more than 98% of the normalized weights; their dependencies on temperature are shown in Figure 3A. The first vector describes a transition with a higher apparent midpoint than that reported by the second vector, analogous with the noncoincident transitions observed for CD and Abs measured at one wavelength (Figure 2B). This qualitative evidence for a multistate unfolding model is supported by the requirement of three basis vectors, implying that a minimum of three states must be involved. The SVD vectors exhibit no dependence on protein concentration in the range of 2.5−20 mM, suggesting that the multistate behavior is not an effect of reversible protein aggregation. This conclusion is further supported by equilibrium sedimentation data that are described well by the presence of a unique monomeric species (data not shown), even after maintaining the protein at 40 °C for 44 h.

SVD analysis of the Abs and Flu spectra recorded during the temperature-induced unfolding in the absence of urea provides vectors with properties (data not shown) similar to those obtained from the decomposition of CD data. The temperature range of transitions for the SVD vectors obtained from Abs is the same as that observed for the CD vectors, but the transition described by the major Abs SVD vector occurs at a lower temperature compared to the second vector. Although the fluorescence data clearly indicate the presence of a hyperfluorescent intermediate (Figure 2C), the large and nonlinear dependence of the native and unfolded baselines on temperature precluded a quantitative analysis of the Flu data.

The three-state character of the unfolding reaction was further investigated by performing temperature-induced unfolding of AS-DHFR in the presence of 0.5, 1.0, 1.5, 2.0, and 2.5 M urea. For the thermal unfolding reaction below 1.5 M urea, the observation of three significant basis vectors implies that a three-state model is required. The two-state versus three-state choice is ambiguous for the temperature-induced unfolding at 1.5 and 2 M urea, and the two-state model is the best choice for the thermal unfolding reaction in 2.5 M urea. A graphical illustration of the convergence from a three-state to a two-state process is provided in Figure 3. The midpoints for the first and second SVD vectors from the thermal melting profiles converge as the urea concentration is increased (Figure 3A−F). Moreover, the amplitude of the unfolding transition monitored by the second vector

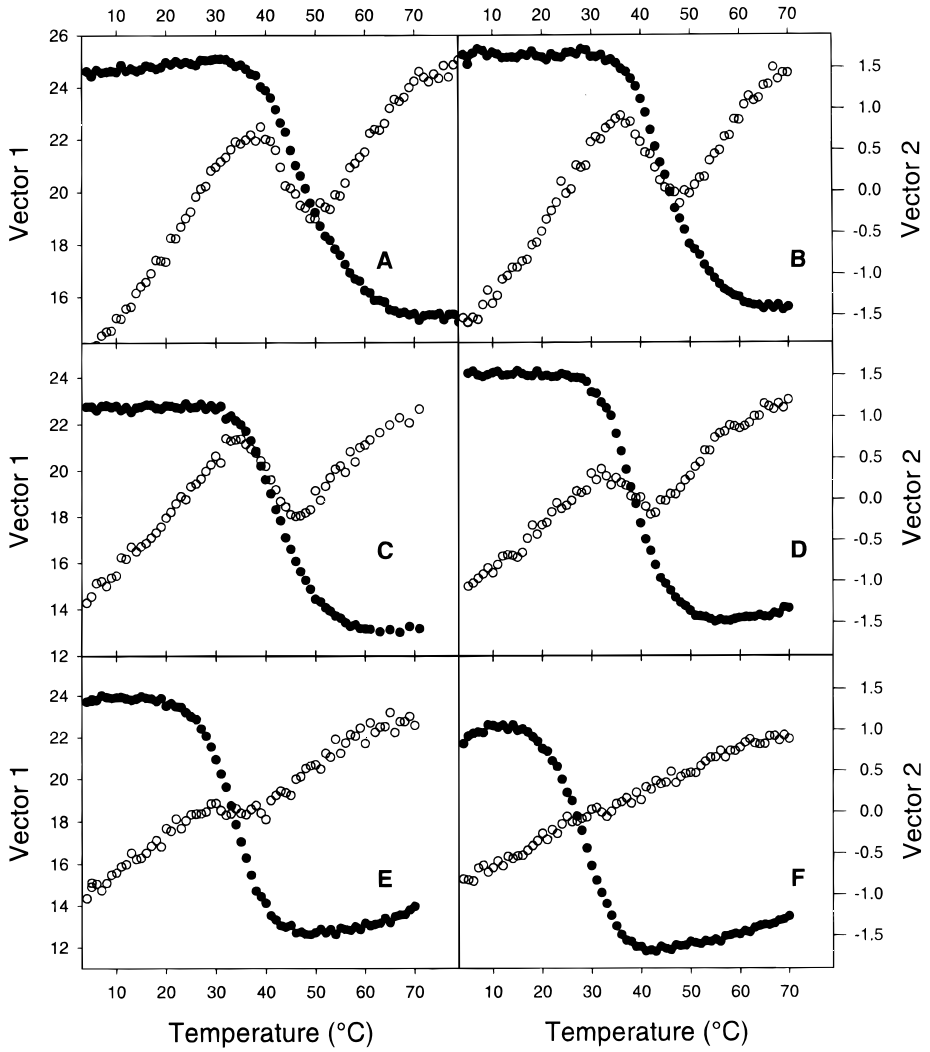

FIGURE 3: First two representative vectors produced by the SVD analysis of the CD spectra as a function of temperature. Vector 1 (●, weight w_1) and vector 2 (○, weight w_2) are shown for the temperature-induced unfolding in the presence of 0 M urea (A; $w_1 = 93\%$, $w_2 = 5\%$), 0.5 M urea (B; $w_1 = 95\%$, $w_2 = 4\%$), 1 M urea (C; $w_1 = 96\%$, $w_2 = 3\%$), 1.5 M urea (D; $w_1 = 96\%$, $w_2 = 3\%$), 2 M urea (E; $w_1 = 96\%$, $w_2 = 3\%$), and 2.5 M urea (F; $w_1 = 96\%$, $w_2 = 3\%$).

diminishes in the presence of increasing urea, and the transition is barely distinguishable from the baselines in 2.5 M urea (Figure 3F). Note that the rollover in the principal vector between 5 and 20 °C at 2.5 M urea reflects cold denaturation (Figure 3F). The convergence of the temperature-induced unfolding from a three-state process to a two-state process in the presence of urea was also observed for SE-DHFR (J. Luo and C. R. Matthews, unpublished results).

Multiple Native Conformers. The relationship of the previously discovered pair of native species (*15*) with the three-state behavior observed for the temperature-induced unfolding of AS-DHFR in the absence of urea was probed by ligand binding studies. The equilibrium between the two native-like species (*15*, *27*) can be determined from the relative amplitudes of the fast (bimolecular) and slow (unimolecular) fluorescence phases accompanying $NADP^+$ binding. The temperature dependence of the populations of two native isoforms of AS-DHFR is shown in Figure 4. The fraction of the $NADP^+$-binding species decreases linearly from 82 to 63% as the temperature increases from 5 to 35 °C. From the temperature dependence of the equilibrium constant K (defined as $K = N_B/N_{NB}$, where N_B and N_{NB} are the concentration of the binding and nonbinding species,

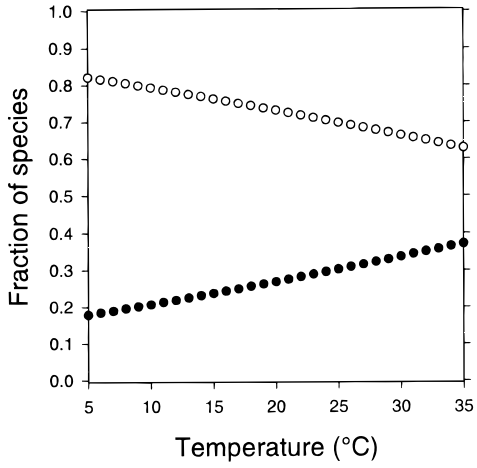

FIGURE 4: Temperature dependence of the fraction of the two native isoforms: N_B (○), the form that binds $NADP^+$, and N_{NB} (●), the nonbinding native species, as determined in stopped-flow fluorescence binding experiments. The protein concentration was 1 μM, and the $NADP^+$ concentration was 100 μM. The buffer was 10 mM potassium phosphate (pH 7.8) with 0.2 mM K_2EDTA.

respectively), the enthalpy and entropy changes at the melting temperature ($T_m = 54$ °C) were calculated to be −5.6 kcal

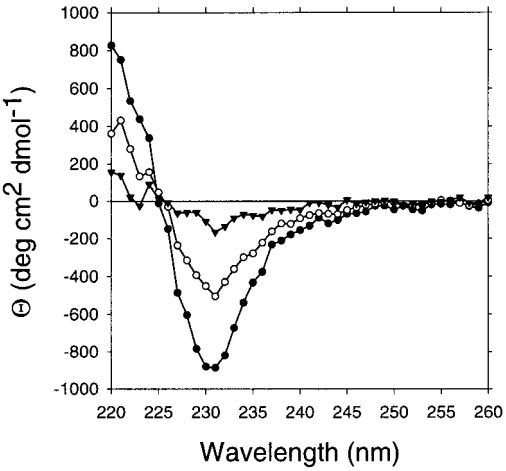

FIGURE 5: Difference spectra determined between CD spectra recorded at several temperatures (▼, 15 °C; ○, 20 °C; ●, 30 °C) and the spectrum recorded at 5 °C. The spectra were collected over a temperature range where the native state predominates (Figure 2). The isodichroic point near 225 nm demonstrates that the changes reflect the interconversion of two species. The experimental conditions are described in the legend of Figure 2.

mol^{-1} and −17 cal mol^{-1} K^{-1}, respectively. The absence of curvature in the plot of the logarithm of the equilibrium constant versus temperature (data not shown) suggests that the difference in heat capacity between the two isoforms is very small. Similar results were reported in a recent study of ligand binding for WT-DHFR (*20*).

In contrast, NADP$^+$ binding studies performed at 20 °C with different urea concentrations of ≤2 M showed no dependence of either the equilibrium between the native-like species or their interconversion rate on denaturant concentration (data not shown). A lack of dependence on urea concentration for the NADP$^+$ binding kinetics was also reported for WT-DHFR (*20*).

Insights into the structural differences between the native conformers can be obtained by examining the native baseline region of AS-DHFR. Difference CD spectra obtained by subtracting the CD spectrum at 5 °C from the CD spectra recorded at ≤35 °C are shown in Figure 5. The minimum at ∼230 nm, null at ∼225 nm, and increase at <225 nm are similar to those observed for the difference CD spectrum between W74L DHFR (a mutant of DHFR with Trp 74 replaced with Leu) and WT-DHFR (*10*). In the latter case, the difference spectrum was attributed to the loss of an exciton coupling between Trp 47 and Trp 74. The data in Figure 5 suggest that the relative populations of the two native species change with temperature in a way that disfavors the exciton-containing species at high temperatures.

Additional evidence that the temperature baseline changes are due to the interconversion between two species was obtained by measuring the CD signal within the same temperature range in the presence of excess NADP$^+$. The absence of change (data not shown) is consistent with the selective stabilization of the active enzyme conformer by NADP$^+$. Native state heterogeneity of WT-DHFR, detected by NMR peak doubling, was also seen to vanish in the presence of folate (*45*).

Urea-Induced Unfolding at Different Temperatures. Urea-induced unfolding of AS-DHFR was assessed at a series of temperatures between 10 and 40 °C. Urea-induced CD or

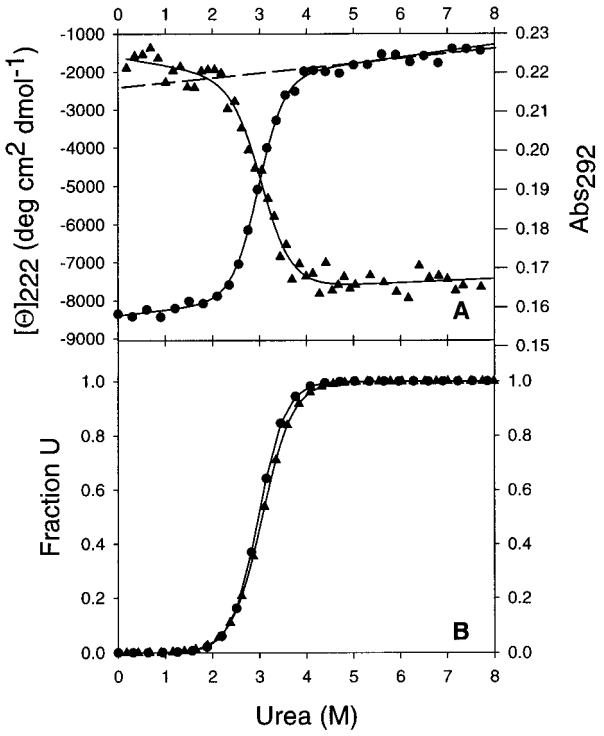

FIGURE 6: (A) AS-DHFR urea-induced unfolding at 20 °C monitored by $[\theta]_{222}$ (●) and Abs_{292} (▲). The solid lines represent the fits obtained by analyzing separately the unfolding profiles with a two-state model. The dashed line represents the linear extrapolation of the CD signal of the unfolded state to 0 M urea. (B) Fraction of the unfolded species obtained from the two-state fits for CD (●) or Abs (▲). The experimental conditions are described in the legend of Figure 2.

Abs unfolding profiles at 20 °C and the corresponding two-state fits are shown in Figure 6A. The two-state character of the transition is supported by the observation that the unfolding transitions are, within experimental errors, coincident (Figure 6B), and by the requirement for only two basis vectors in the SVD analysis at all temperatures that were examined. The cooperativity of the urea-induced transition (as indicated by the *m* value in a two-state fit) is constant up to 30 °C (2 kcal mol^{-1} M^{-1}), but decreases significantly at higher temperatures (1.3 kcal mol^{-1} M^{-1} at 40 °C). A similar dependence on temperature was reported recently for the *m* value of WT-DHFR (*20*). The significant decrease in the *m* value suggests that an intermediate state becomes significantly populated with increasing temperatures.

Global Analysis. The minimal model required to describe the temperature- and urea-induced unfolding of AS-DHFR involves three thermodynamic states: native (N), intermediate (I), and unfolded (U). Although the ligand binding data clearly demonstrate the presence of two native conformers, their structural and thermodynamic properties are sufficiently similar that the application of a four-state model, $N_B \rightleftarrows N_{NB} \rightleftarrows I \rightleftarrows U$, does not improve the goodness of the fit. With this limitation, the thermodynamic parameters extracted from the three-state analysis must be considered as "apparent" parameters. As such, they represent average values whose weights reflect the relative populations of the N_{NB} and N_B states. The data incorporated into the global analysis included the first three vectors obtained by SVD analysis of CD and Abs spectra obtained during both temperature- and urea-induced unfolding. Only the fluorescence data for urea-

Table 1: Thermodynamic Parameters for the Unfolding of AS-DHFR[a]

	N ⇄ I	I ⇄ U	N ⇄ U
T_m (°C)	46 ± 1	59 ± 2	N/A
$\Delta S_m°$ (cal mol^{-1} K^{-1})	186 ± 20	147 ± 22	N/A
$\Delta H_m°$ (kcal mol^{-1})	59 ± 7	49 ± 7	N/A
ΔC_p (kcal mol^{-1} K^{-1})	0.9[b]	1.6[c]	2.50 ± 0.25[b]
m (kcal mol^{-1} M^{-1})	0.7 ± 0.2	1.25[c]	1.95 ± 0.10

[a] The standard deviations were determined by a rigorous error analysis (*58*). Although the errors recovered from this analysis are not symmetric, the differences between the lower and the upper limit are not large. The values shown represent their average. [b] ΔC_{p-NI} was calculated with the equation $\Delta C_{p-NI} = \Delta C_{p-NU}(m_{NI}/m_{NU})$. Only the total change in heat capacity upon unfolding was used as a fitting parameter in the global analysis. [c] The values for the I ⇄ U transition were calculated as the difference between the values for the N ⇄ U and N ⇄ I transitions.

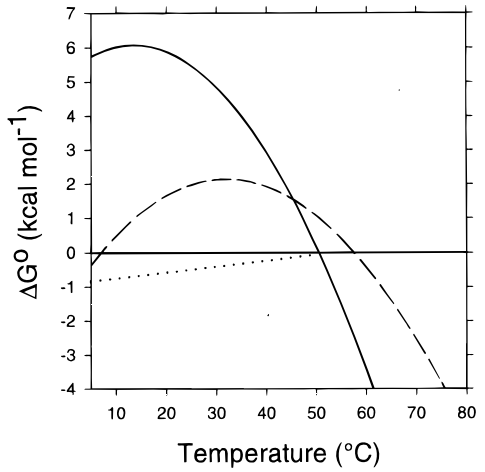

FIGURE 7: Temperature dependence of the free energy difference between native and unfolded (solid line) and between intermediate and unfolded (dashed line) states of AS-DHFR at pH 7.8. The free energy difference between N_{NB} and N_B forms (dotted line) was determined by NADP$^+$ binding experiments.

induced unfolding were included in the data pool because the extreme slope of the baselines for the thermal transition precluded a reliable analysis.

The thermodynamic parameters obtained from the global analysis are presented in Table 1. The melting temperatures for the transitions between N and I and between I and U are 46 and 59 °C, respectively. The corresponding entropies of unfolding are 186 and 147 cal mol^{-1} K^{-1}, and the enthalpies of unfolding are 59 and 49 kcal mol^{-1}. The *m* value and heat capacity change for complete unfolding are 2.0 kcal mol^{-1} M^{-1} and 2.5 kcal mol^{-1} K^{-1}, respectively, and are consistent with the values expected for a globular protein of this size (*44*). If it is assumed that the *m* value reflects the changes in buried surface area (*44*), the majority of the buried surface area is exposed in the I ⇄ U transition.

The temperature dependence of the apparent free energy of folding for AS-DHFR in the absence of urea is shown in Figure 7. The maximum stability of 6 kcal mol^{-1} at 15 °C is in good agreement with several previous estimations of WT and AS-DHFR stabilities (*12*, *19*), but differs by ~2 kcal mol^{-1} from a more recent estimation for WT-DHFR (*20*). The intermediate has a maximum stability of ~2 kcal mol^{-1} at 32 °C and becomes more stable than the native form at 45 °C. At temperatures of >60 °C, the unfolded state is the most stable species. Also shown in Figure 7 is the difference in free energy between the two isoforms of the native state. A difference of less than 1 kcal mol^{-1} over the temperature range that was investigated accounts for the goodness of the fit to a model that postulates a single native state.

The fractions of the species involved in the folding of AS-DHFR are shown in Figure 8 along both temperature and urea axes. The fractions of two native isoforms were calculated from the equilibrium constant determined from ligand binding experiments and the total native state fraction from the three-state global analysis. The native state ensemble (dominated by the NADP$^+$ binding form) is highly populated below 35 °C and up to 3 M urea. The population of the intermediate is negligible (less than 10%) at temperatures of <35 or >65 °C at any urea concentration; the maximal population is about 70% at 50 °C. The intermediate is also negligible at any temperature for urea concentrations of >2 M. In the high-temperature, high-urea concentration range, the unfolded state becomes the predominant species.

DISCUSSION

The global analysis of the temperature- and urea-induced unfolding of AS-DHFR monitored by Abs, Flu, and CD spectroscopy requires a minimum of three thermodynamic states whose spectroscopic properties support their designation as native, intermediate, and unfolded states.

Native State Ensemble. It has long been known that the native state of DHFR from both prokaryotic and eukaryotic sources is comprised of at least two slowly interconverting conformations with different affinities for substrate and cofactor (*15*, *20*, *27*). The kinetic folding model (*13*) also postulates a role for multiple native forms in both the unfolding and refolding reactions. Although the source of the structural heterogeneity is not known, a recent X-ray analysis of a series of DHFR−ligand complexes (*9*) suggests that different docking modes between the loop and nucleotide-binding domains may be involved. Doubling of many of the side chain resonances in the two-dimensional NMR spectrum of WT-DHFR (*16*) revealed that the heterogeneity is not localized but distributed across most, if not all, of the protein. Thus, the observation that the temperature- and urea-induced unfolding reactions of AS-DHFR are described well by a thermodynamic model that only involves a single native state requires an explanation.

A resolution for the apparent discrepancy can be found in the results of NADP$^+$ binding experiments in the native baseline regions along both denaturation axes. The weak temperature dependence and the absence of a urea dependence between the minor, N_{NB}, and major, N_B, conformations make it impossible to resolve their independent contributions from simple baseline effects expected for protein unfolding reactions. The failure to improve the quality of the fit of the data with a four-state model involving two native states (data not shown) is consistent with this interpretation and with the small free energy difference between these states (Figure 7).

The small but measurable enthalpy difference between N_{NB} and N_B is, however, useful in highlighting a structural difference between these two members of the native ensemble. The far-UV CD difference spectrum in the thermal

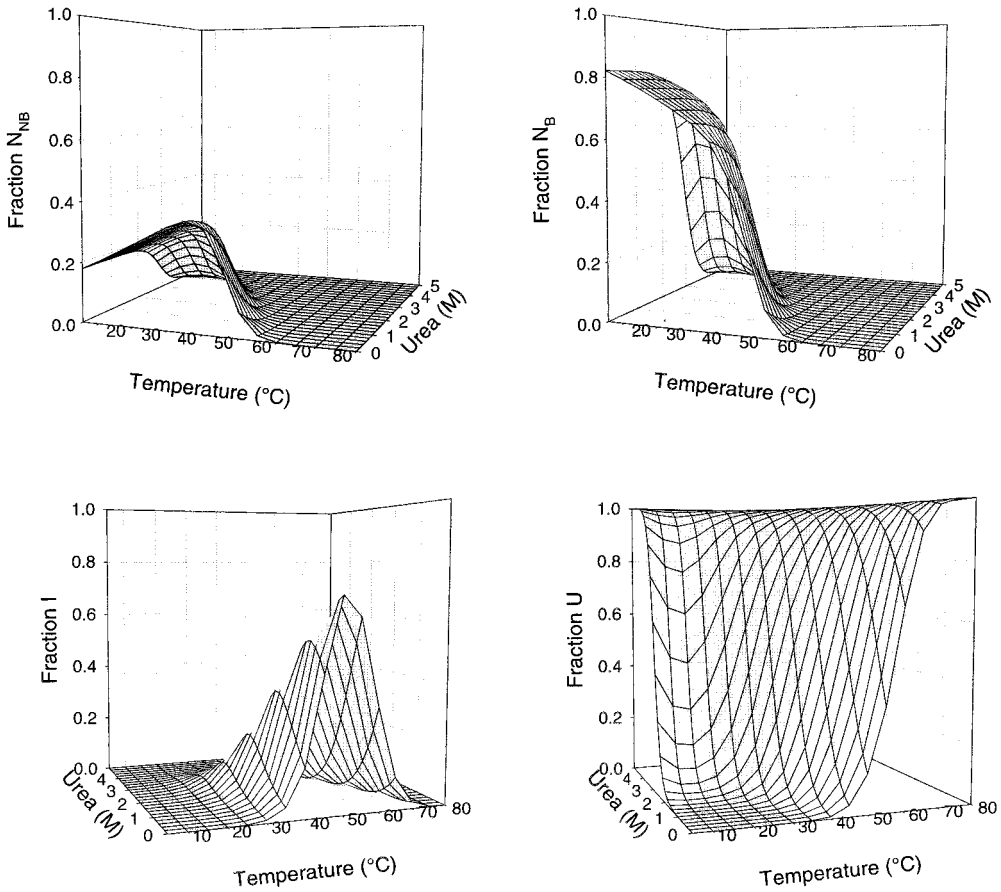

FIGURE 8: Fraction of the population of the N_{NB}, N_B, I, and U species as a function of urea concentration and temperature at pH 7.8.

baseline region (Figure 5) is very similar to the difference spectrum between WT and W74L DHFR (*10*). This symmetric difference spectrum was attributed to the loss of an exciton coupling between Trp 47 and Trp 74 in the W74L mutant protein. The increase in the difference spectrum with increasing temperature demonstrates that the conversion of the N_B to N_{NB} state must alter the distance and/or orientation between these two tryptophans in a fashion that diminishes the exciton coupling. By inference, the packing of the nucleotide-binding domain must differ in the two conformers. Although neither of the tryptophan side chains was among those with doubled resonances in the NMR spectrum of DHFR (*16*), subtle changes in orientation may result in minor cross-peaks that could not be unambiguously assigned (C. Falzone, personal communication).

The lack of an effect of urea on the $N_{NB} \rightleftarrows N_B$ equilibrium and the absence of a heat capacity difference for the interconversion reaction implies similar buried surface areas in both states (*44*). Therefore, both states must be folded well, and any changes in packing must conserve buried surface area. These general structural features suggest that the designation of both conformers as being members of the native ensemble is appropriate. In contrast, Clark and Frieden (*20*) used a combined thermodynamic and kinetic analysis to assign the minor, nonligand binding conformer to a late folding intermediate. Although protein may flow through N_{NB} to N_B during folding at very low urea concentrations, the distinct urea dependence of both folding reactions leading to N_{NB} and N_B (*13*) supports the notion that a pair of less well-folded intermediates is the primary precursor to the two native conformers.

Intermediate Ensemble. DHFR is thought to refold via two types of kinetic intermediates (*13*); one forms within the instrument dead time, 5 ms, and a subsequent type becomes populated in the first few hundred milliseconds of refolding. The burst phase intermediate, observed by CD (*10*) and pulse-labeling hydrogen NMR (*46*) methods, but *not* by fluorescence (*11*), is a marginally stable, compact state (*47*). The topology of the native fold is established for a major fraction, but not all, of the population of this early intermediate (*46*). The subsequent intermediate has greater fluorescence intensity than that of the native or the unfolded states (*12*); the enhanced intensity has been shown to reflect the burial of Trp 74 in a hydrophobic cluster (*11*). Complementary experiments have shown that this intermediate is not able to bind methotrexate (*13*, *46*), even though Trp 47 and Trp 74 are in a favorable orientation for exciton coupling (*10*). The folding of this hyperfluorescent intermediate to four native-like forms occurs via four exponential processes whose amplitudes are not proportional to the relative rate constants. Thus, the intermediate ensemble must be comprised of four, slowly interconverting species that fold to the native ensemble through parallel channels.

On the basis of its spectroscopic properties, the equilibrium intermediate ensemble more closely resembles the set of intermediates that appears after a few hundred milliseconds and not the burst phase species. Thus, the thermodynamic properties reported for the equilibrium intermediate may reflect the average properties of the set of four hyperfluorescent intermediates. Because the burial of Trp 74 follows the same time course as the development of the exciton coupling in the far-UV CD spectrum (*10*), it is

possible that the nucleotide-binding domain is largely folded in the equilibrium intermediate. This view is supported by the observation of native-like packing around Ile 91 in the burst phase intermediate. Ile 91 is a part of a hydrophobic cluster on the opposing face of the α-sheet in the nucleotide-binding domain (*48*). Although a fragment corresponding to this domain does not adopt a stable fold (*49*), the domain may, in the context of the remainder of the sequence for AS-DHFR, play an important role in guiding its folding along the free energy surface for the reaction. The very common occurrence of nucleotide-binding domains in proteins (*50*, *51*) suggests that these motifs may play similar roles in the folding of a large number of proteins.

Unfolded State Ensemble. The goodness of fit of a three-state equilibrium model that only involves a single unfolded form implies that the thermally and urea-denatured forms are thermodynamically equivalent. The absence of a cooperative thermal transition for the urea-denatured form or a cooperative urea-induced transition for the thermally denatured form (data not shown) provides further support for the contention that both denatured forms are part of the same unfolded thermodynamic state. However, linear extrapolation of the far-UV CD unfolded baselines for AS-DHFR to native conditions, 0 M urea (Figure 6) and 20 °C (Figure 2), shows that the amplitude of the signal for the thermally denatured form is substantially greater than that for the urea-denatured form. Although the proper form of the extrapolation required to make this comparison is a matter of debate (*52*, *53*), the linear extrapolation for DHFR is consistent with the behavior of short peptides (data not shown) and of fragments of DHFR (*49*). If the larger signal for the thermally denatured form reflects the presence of a greater amount of secondary structure, then the ensemble of structures representing the unfolded thermodynamic state is sufficiently broad to encompass species with a range of residual secondary structure.

The observation that the thermally and chemically denatured forms of DHFR are spectroscopically distinct is similar to the observations made for several other proteins, including lysozyme (*54*, *55*) and cytochrome *c* (*56*). In contrast, the temperature- and urea-induced unfolded states are thermodynamically and spectroscopically equivalent for λ-repressor (*31*), HPr (*33*), and barstar (*36*).

It is possible that two or more thermodynamic states exist in the denatured baseline region for AS-DHFR. If these states only differ marginally in their thermodynamic properties, they would be difficult to resolve by standard titration methods. This explanation is supported by the results of kinetic studies on the refolding of urea-denatured DHFR. At least two different conformations appear within the first few milliseconds of the reaction (*46*). These conformers could reflect distinct populations of unfolded forms that interconvert more slowly than they fold to the set of burst phase intermediates. Double-jump experiments rule out cis−trans proline isomerization as the source of heterogeneity in the unfolded state (*13*). Support for the notion of multiple unfolded states in DHFR is also provided by the results of ^{19}F NMR spectroscopy studies on 6-fluorotryptophan-labeled WT-DHFR in 7.8 M urea. Three out of five ^{19}F resonances (positions 22, 74, and 133) have chemical shifts distinct from that of free 6-fluorotryptophan (*57*). Although the shifts were attributed to local sequence effects, localized residual structure with a substantial barrier might serve as the source for multiple unfolded states and parallel folding channels.

Summary. The insights into the structural and thermodynamic properties of a stable partially folded form for AS-DHFR highlight the power of the global thermodynamic analysis. The correspondence between this equilibrium intermediate and a set of four, closely related, transient folding intermediates suggests that, at least for the later stages of folding, the thermodynamic properties of this system are an important determinant of the kinetic mechanism. The limitations of the approach are made evident by the ligand binding experiments that reveal the presence of at least two native-like forms, one which does and one which does not bind $NADP^+$. The combination of equilibrium and kinetic data into a complete global analysis of the folding reaction of AS-DHFR may allow us to overcome this limitation and define a detailed energy surface for this complex process. These efforts are now in progress.

ACKNOWLEDGMENT

The previous work of Dr. Jaibin Luo on SE-DHFR was the impetus for these studies. We acknowledge his contribution to the understanding of the thermodynamic and spectroscopic properties of DHFR variants. We thank Dr. Osman Bilsel for helpful discussions regarding the data analysis and Drs. Jill A. Zitzewitz and Beatriz Ibarra-Molero for advice and critical review of the manuscript.

REFERENCES

1. Anfinsen, C. B. (1973) *Science 181*, 223−230.
2. Bilsel, O., Zitzewitz, J. A., Bowers, K. E., and Matthews, C. R. (1999) *Biochemistry 38*, 1018−1029.
3. Eftink, M. R., and Ionescu, R. M. (1997) *Biophys. Chem. 64*, 175−197.
4. Dill, K. A., and Shortle, D. (1991) *Annu. Rev. Biochem. 60*, 795−825.
5. Zhou, Y., Hall, C. K., and Karplus, M. (1999) *Protein Sci. 8*, 1064−1074.
6. Gualfetti, P. J., Bilsel, O., and Matthews, C. R. (1999) *Protein Sci. 8*, 1623−1635.
7. Gloss, L. M., and Matthews, C. R. (1997) *Biochemistry 36*, 5612−5623.
8. Ionescu, R. M., and Eftink, M. R. (1997) *Biochemistry 36*, 1129−1140.
9. Sawaya, M. R., and Kraut, J. (1997) *Biochemistry 36*, 586−603.
10. Kuwajima, K., Garvey, E. P., Finn, B. E., Matthews, C. R., and Sugai, S. (1991) *Biochemistry 30*, 7693−7703.
11. Garvey, E. P., Swank, J., and Matthews, C. R. (1989) *Proteins: Struct., Funct., Genet. 6*, 259−266.
12. Touchette, N. A., Perry, K. M., and Matthews, C. R. (1986) *Biochemistry 25*, 5445−5452.
13. Jennings, P. A., Finn, B. E., Jones, B. E., and Matthews, C. R. (1993) *Biochemistry 32*, 3783−3789.
14. Jones, B. E., Jennings, P. A., Pierre, R. A., and Matthews, C. R. (1994) *Biochemistry 33*, 15250−15258.
15. Cayley, P. J., Dunn, S. M. J., and King, R. W. (1981) *Biochemistry 20*, 874−879.
16. Falzone, C. J., Wright, P. E., and Benkovic, S. J. (1991) *Biochemistry 30*, 2184−2191.
17. Uedaira, H., Kidokoro, S., Iwakura, M., Honda, S., and Ohashi, S. (1990) *Thermochim. Acta 163*, 123−128.
18. Ohmae, E., Kurumiya, T., Makino, S., and Gekko, K. (1996) *J. Biochem. 120*, 946−953.
19. Iwakura, M., Jones, B. E., Luo, J., and Matthews, C. R. (1995) *J. Biochem. 117*, 480−488.
20. Clark, A. C., and Frieden, C. (1999) *J. Mol. Biol. 285*, 1765−1776.

21. Pace, C. N. (1986) *Methods Enzymol. 131*, 266−280.
22. Jennings, P. A., and Wright, P. E. (1993) *Science 262*, 892−896.
23. Johnson, M. L., and Fraiser, S. G. (1985) *Methods Enzymol. 117*, 301−342.
24. NONLIN available from http://www.bbri.org/rasmb/rasmb.html.
25. Philo, J., Haynes, D. B., and Laue, T. M. (1997) SEDENTERP, available from http://www.bbri.org/rasmb/spin/spin.html.
26. Laue, T. M., Shah, B., Ridgeway, T. M., and Pelletier, S. L. (1992) in *Analytical Ultracentrifugation in Biochemistry and Polymer Science* (Harding, S. E., Horton, J. C., and Rowe, A. J., Eds.) pp 90−125, Royal Society of Chemistry, Cambridge, U.K.
27. Dunn, S. M. J., Batchelor, J. G., and King, R. W. (1978) *Biochemistry 17*, 2356−2364.
28. Frieden, C. (1990) *Proc. Natl. Acad. Sci. U.S.A. 87*, 4413−4416.
29. Henry, E. R., and Hofrichter, J. (1992) *Methods Enzymol. 210*, 129−192.
30. Luo, J., Iwakura, M., and Matthews, C. R. (1995) *Biochemistry 34*, 10669−10675.
31. Huang, G. S., and Oas, T. G. (1996) *Biochemistry 35*, 6173−6180.
32. Chen, B., and Schellman, J. A. (1989) *Biochemistry 28*, 685−691.
33. Scholtz, J. M. (1995) *Protein Sci. 4*, 35−43.
34. Swint, L., and Robertson, A. D. (1993) *Protein Sci. 2*, 2037−2049.
35. Hu, C., Sturtevant, J. M., Thomson, J. A., Erickson, R. E., and Pace, C. N. (1992) *Biochemistry 31*, 4876−4882.
36. Agashe, V. R., and Udgaonkar, J. B. (1995) *Biochemistry 34*, 3286−3299.
37. Villegas, V., Azuaga, A., Catasus, L., Reverter, D., Mateo, P. L., Aviles, F. X., and Serrano, L. (1995) *Biochemistry 34*, 15105−15110.
38. Chiti, F., van Nuland, N. A. J., Taddei, N., Magherini, F., Stefani, M., Ramponi, G., and Dobson, C. M. (1998) *Biochemistry 37*, 1447−1455.
39. Taddei, N., Chiti, F., Paoli, P., Fiaschi, T., Bucciantini, M., Stefani, M., Dobson, C. M., and Ramponi, G. (1999) *Biochemistry 38*, 2135−2142.
40. Kuhlman, B., and Raleigh, D. P. (1998) *Protein Sci. 7*, 2405−2412.
41. Nicholson, E. M., and Scholtz, J. M. (1996) *Biochemistry 35*, 11369−11378.
42. Gomez, J., Hilser, V. J., Xie, D., and Freire, E. (1995) *Proteins: Struct., Funct., Genet. 22*, 404−412.
43. Privalov, P. L. (1979) *Adv. Protein Chem. 33*, 167−241.
44. Robertson, A. D., and Murphy, K. P. (1997) *Chem. Rev. 97*, 1251−1267.
45. Falzone, C. J., Benkovic, S. J., and Wright, P. E. (1990) *Biochemistry 29*, 9667−9677.
46. Jones, B. E., and Matthews, C. R. (1995) *Protein Sci. 4*, 167−177.
47. Jones, B. E., Beechem, J. M., and Matthews, C. R. (1995) *Biochemistry 34*, 1867−1877.
48. O'Neill, J. C., and Matthews, C. R. (2000) *J. Mol. Biol. 295*, 737−744.
49. Gegg, C. V., Bowers, K. E., and Matthews, C. R. (1997) *Protein Sci. 6*, 1885−1892.
50. Teichmann, S. A., Chothia, C., and Gerstein, M. (1999) *Curr. Opin. Struct. Biol. 9*, 390−399.
51. Thornton, J. M., Orengo, C. A., Todd, A. E., and Pearl, F. M. (1999) *J. Mol. Biol. 293*, 333−342.
52. Qi, P. X., Sosnick, T. R., and Englander, S. W. (1998) *Nat. Struct. Biol. 5*, 882−884.
53. Baskakov, I. V., and Bolen, D. W. (1998) *Biochemistry 37*, 18010−18017.
54. Ikeguchi, M., Kuwajima, K., Mitani, M., and Sugai, S. (1986) *Biochemistry 25*, 6965−6972.
55. Kuwajima, K., Hiraoka, Y., Ikeguchi, M., and Sugai, S. (1985) *Biochemistry 24*, 874−881.
56. Hagihara, Y., Tan, Y., and Goto, Y. (1994) *J. Mol. Biol. 237*, 336−348.
57. Hoeltzli, S. D., and Frieden, C. (1994) *Biochemistry 33*, 5502−5509.
58. Beechem, J. M., Gratton, E., Ameloot, M., Knutson, J. R., and Brand, L. (1991) in *Topics in Fluorescence Spectroscopy* (Lakowicz, J. R., Ed.) Vol. 2, pp 241−306, Plenum Press, New York.
59. Kraulis, P. J. (1991) *J. Appl. Crystallogr. 24*, 946−950.

BI000511Y